Design and simulation of waveguide-integrated Ge/SiGe quantum-confined Stark effect optical modulator based on adiabatic coupling with SiGe waveguide

Worawat Traiwattanapong, (iD) **Papichaya Chaisakul,** (iD) **Jacopo Frigerio, Daniel Chrastina,** (iD) **Giovanni Isella,**
Laurent Vivien, and (iD) **Delphine Marris-Morini**

Design and simulation of waveguide-integrated Ge/SiGe quantum-confined Stark effect optical modulator based on adiabatic coupling with SiGe waveguide

View Online   Export Citation   CrossMark

Worawat Traiwattanapong,[1] Papichaya Chaisakul,[1,a] (iD) Jacopo Frigerio,[2] (iD) Daniel Chrastina,[2]
Giovanni Isella,[2] (iD) Laurent Vivien,[3] and Delphine Marris-Morini[3] (iD)

AFFILIATIONS

[1] Department of Physics, Faculty of Science, Kasetsart University, Bangkok 10900, Thailand
[2] L-NESS, Dipartimento di Fisica, Politecnico di Milano, Polo di Como, ViaAnzani 42, 22100 Como, Italy
[3] Centre de Nanosciences et de Nanotechnologies, Université Paris Sud, CNRS, Université Paris Saclay, 91120 Palaiseau, France

[a]Author to whom correspondence should be addressed: fscipac@ku.ac.th

ABSTRACT

We report on the design and simulation of a waveguide-integrated Ge/SiGe quantum-confined Stark effect (QCSE) optical modulator based on the use of a Ge-rich SiGe relaxed buffer on a graded buffer as an optical waveguide. Despite the promising potential of this waveguide platform, efficient and wideband optical integration with a Ge-based active device has not been properly addressed so far. In this paper, via 3D finite-difference time domain simulation, we demonstrate that a simple 2D taper is sufficient to enable adiabatic optical coupling from the fundamental mode of the input SiGe waveguide to the fundamental mode of the Ge/SiGe multiple quantum well (MQW) modulator without the excitation of higher-order modes in Ge/SiGe MQWs. The 2D taper shows good fabrication tolerance considering critical variations in its dimensions. Significantly, wideband optical modulation performance in terms of extinction ratio and insertion loss is presented over the whole low-loss spectral range of the Ge/SiGe MQWs at different electrical bias values, device lengths, and numbers of quantum wells in order to comprehensively report its potential for Si-based optical modulators.

I. INTRODUCTION

Quantum-confined Stark effect (QCSE) from germanium /silicon–germanium multiple quantum wells (Ge/SiGe MQWs) has been regarded as one of the strongest physical mechanisms to obtain a group-IV optical modulator, which could be fabricated using top-down optical lithography and dry etching techniques. Since the discovery of strong QCSE from the direct-gap transition of Ge/SiGe MQWs at room temperature,[1] various theoretical and experimental works have been performed to gain an understanding on the material systems and develop compact and low-voltage waveguide-integrated Si-based optical modulators within the telecommunication wavelength regions from O-band to C-band (1260 nm–1550 nm).[2–19] Si-based optical interconnect is one of the promising options to support the economic and environmental sustainability of growth in data transmission needed for the projected expansion of communication, commerce, and computation.[20–22] The optical integration between silicon-on-insulator (SOI) waveguide and Ge/SiGe MQWs has been widely investigated both theoretically and experimentally in order to realize Si-based waveguide-integrated optical modulators on the SOI platforms using either eigenmode expansion method simulations or optical transmission measurements.[16–19] Recently, Zang et al.[23] have theoretically shown from finite-difference time domain (FDTD) simulations that for the optical integration with the SOI waveguide, using a 2D taper (tapering in the direction horizontal to the plane of the wafer) might not be sufficient to suppress the excitation of the higher-order modes inside the Ge/SiGe MQW optical modulator, and a 3D taper

(tapering in directions horizontal and vertical to the plane of the wafer) is required. Nevertheless, although 3D tapers may be superior to 2D ones in suppressing the excitation of the higher-order modes in the Ge/SiGe modulator, it should be noted that their realization is not a trivial task using a top-down fabrication process. Indeed, the main reason for the existence of the higher-order mode in the Ge/SiGe modulator is that a Ge-rich SiGe relaxed buffer of several 100 nm thick is typically required to grow Ge/SiGe MQWs to properly compensate the built-in strain in the structures. The excitation of higher-order modes would cause the transmitted power at the modulator output to be length-dependent because of the beating between different co-propagating modes in the Ge/SiGe MQWs section, which would negatively affect the reliability of the device's design and fabrication.[23,24] Recent effort also includes the growth of Ge/SiGe MQWs on a Ge-rich SiGe relaxed buffer as thin as 100 nm to simplify optical integration with the SOI waveguide.[25]

On the other hand, we have proposed and experimentally validated the use of Ge-rich SiGe relaxed buffer as a passive optical waveguide and realized an integrated optical interconnect consisting of waveguide-integrated Ge/SiGe QCSE optical modulator and photodetector on bulk Si wafer.[26] The proof-of-concept device confirmed that Ge-rich SiGe relaxed buffer could be simultaneously used as both a compact and low loss waveguide platform and a virtual substrate (VS) on which high quality epitaxial growth of the Ge/SiGe MQWs could be performed at a relatively low temperature ($\leq 450\,^{\circ}$C) as demonstrated by the good performance of the stand-alone optical modulator and photodetector devices. Moreover, the integrated optical interconnects showed promising potential for low-bit-error-rate (BER) data transmission mainly due to a very low dark current level at the SiGe waveguide-integrated Ge/SiGe photodetector. Nevertheless, the performance of SiGe waveguide-integrated Ge/SiGe QCSE optical modulator was relatively modest and worth further investigation, as the observed 2-dB extinction ratio with ~5-dB insertion loss (including both in- and out-taper coupling and the Ge/SiGe MQW background absorption loss) can be significantly improved. From our FDTD simulation, it was found that such non-optimal modulation performance stemmed from the fact that the other optical modes, besides the fundamental one, were also excited in the proof-of-concept waveguide-integrated Ge/SiGe optical modulator.

As a result, despite the promising potential of Ge-rich SiGe relaxed buffer on SiGe graded buffer waveguide platform for monolithic integration of optical interconnects with bulk Si CMOS,[26] efficient and wideband optical integration with Ge-based active device has not been properly addressed so far. In this paper, via 3D FDTD simulation, we demonstrate that for the proposed SiGe waveguide-integrated Ge/SiGe QCSE optical modulator, a simple 2D taper is sufficient to attain adiabatic optical coupling from the fundamental mode of the input SiGe waveguide to the fundamental mode of the Ge/SiGe MQWs modulator, without the excitation of higher-order modes in Ge/SiGe MQWs. Moreover, the 2D taper shows excellent fabrication tolerance considering possible variations in its dimensions. Significantly, we have also investigated the wideband optical modulation performance of the SiGe waveguide-integrated Ge/SiGe QCSE optical modulator over the whole low-loss spectral range of the Ge/SiGe MQWs under investigation with different values of device's length and numbers of QW layers, in order to

comprehensively report its potential for compact Si-based optical modulator. We might be obliged to point out that our work is different from Ref. 27, in which it focused on only the optical coupling part and the coupler appeared to be resonant-typed (usually based on mode beating); besides, the information on layers' thickness and refractive index were not available in the previous study.

II. $Si_{0.16}Ge_{0.84}$ WAVEGUIDE INTEGRATED $Ge/Si_{0.16}Ge_{0.84}$ MULTI-QUANTUM-WELL

The $Si_{0.16}Ge_{0.84}$ waveguide integrated $Ge/Si_{0.16}Ge_{0.84}$ multi-quantum-well QCSE optical modulator under investigation is illustrated in Fig. 1. Consistent with our first proof-of-concept experimental demonstration in Ref. 26, the first part of the structure is an 8-μm-thick $Si_{1-y}Ge_y$ graded buffer, with a linear increase in Ge concentration y from 0% to 83%, which can be deposited at a relatively fast rate of $5\,\text{nm s}^{-1}$–$10\,\text{nm s}^{-1}$,[28] and a 2-μm-wide, 1.5-μm-high, and 1-μm-etched $Si_{0.16}Ge_{0.84}$ rib waveguide is considered. Despite a low refractive index contrast between the waveguide core and the graded buffer, strong light confinement in the waveguide core can be obtained, as shown in the top-left inset of Fig. 2(a); moreover, we had demonstrated that tight bend radius can be obtained in this waveguide structure.[29] For the Ge/SiGe MQW structures, a 200-nm-thick $Si_{0.09}Ge_{0.91}$ layer is intended for p-type contact; a

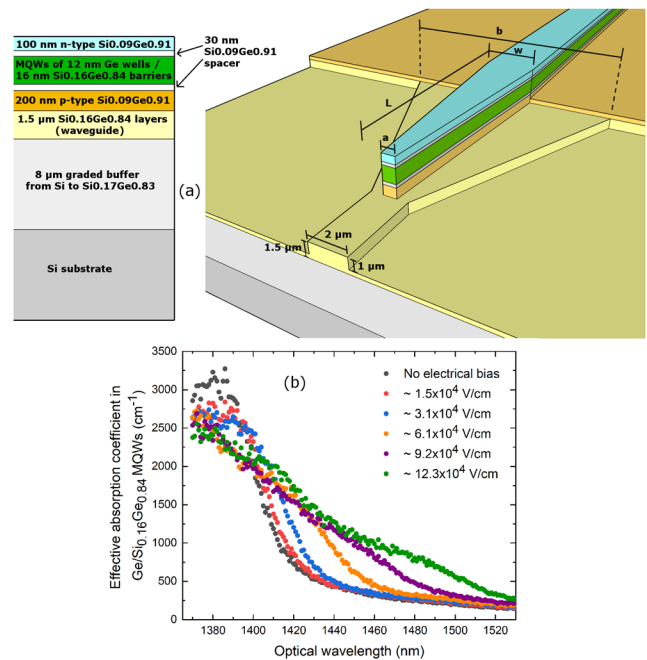FIG. 1. (a) Schematic view of the $Ge/Si_{0.16}Ge_{0.84}$ multi-quantum wells structure and the integration between $Si_{0.16}Ge_{0.84}$ waveguide and $Ge/Si_{0.16}Ge_{0.84}$ multi-quantum wells via the investigated 2D taper with different dimensional parameters. (b) The spectral absorption coefficient values of the $Ge/Si_{0.16}Ge_{0.84}$ MQWs at different electrical bias extracted from the experimental data.[26] For ten QW periods, the optimized values of the taper tip width (a), taper length (L), taper end width (w), and width of $Si_{0.16}Ge_{0.84}$ rib waveguide at the tip of the taper (b) are 0.7 μm, 30 μm, 1.4 μm, and 5.3 μm, respectively.
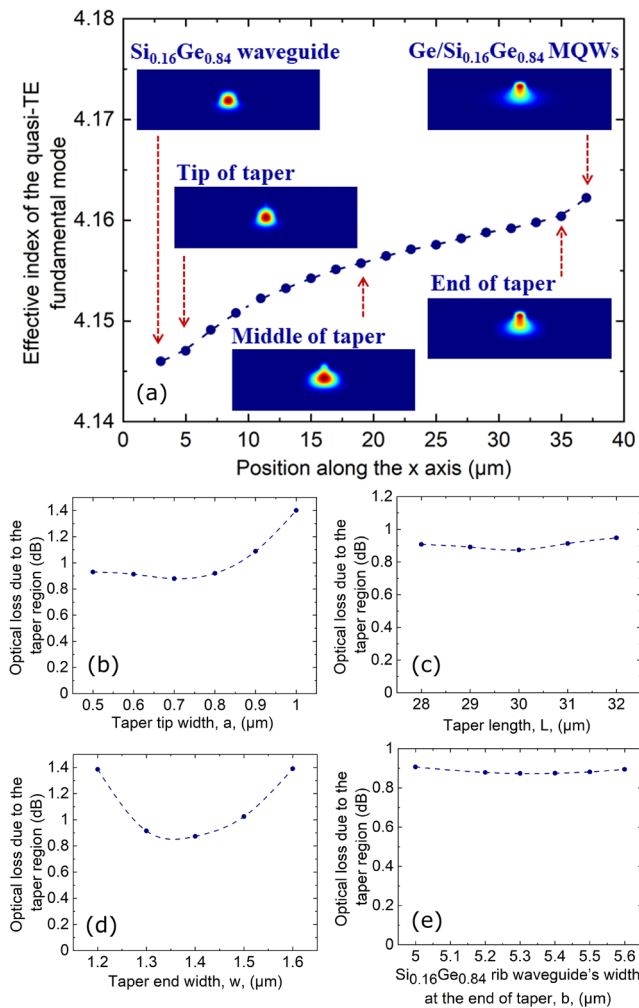
FIG. 2. (a) Effective index of the quasi-TE fundamental at different positions along the propagation axis of the 2D taper from the $Si_{0.16}Ge_{0.84}$ waveguide to the $Ge/Si_{0.16}Ge_{0.84}$ MQW; the corresponding optical mode at selected positions can be seen in the inset. Optical coupling loss between the fundamental quasi-TE mode at the $Si_{0.16}Ge_{0.84}$ waveguide and the fundamental quasi-TE mode at the end of taper with respect to the variations in (b) taper tip width, (c) taper length, (d) taper end width, and (e) $Si_{0.16}Ge_{0.84}$ rib waveguide's width at the end of the taper.

subtle but crucial point in the modulator design is that the p-type layer needs to be partially etched to take into account the p-type contact. This is followed by a 30-nm-thick $Si_{0.09}Ge_{0.91}$ spacer, while the MQW itself consists of ten (different numbers of QW periods will be investigated later) periods of 12-nm-thick Ge QWs separated by 16-nm-thick $Si_{0.16}Ge_{0.84}$ barriers, resulting in an average Ge content of ~91%, on which a 30-nm-thick $Si_{0.09}Ge_{0.91}$ spacer and a 100-nm-thick n-doped $Si_{0.09}Ge_{0.91}$ layer are, respectively, employed to allow the application of electric fields in the MQW region. Different from the proof-of-concept device, after optimization we have arrived at a 2D taper with a tip width (a) of 0.7 μm, a length (L) of 30 μm, and an end width (w) of 1.4 μm, which equals to the width of the Ge/SiGe MQW waveguide section. The width of $Si_{0.16}Ge_{0.84}$ rib waveguide

should be expanded from 2 μm at the tip of the taper to 5.3 μm at the end of the taper. The refractive index of $Si_{1-y}Ge_y$ is assumed to be a linear variation between those of Ge (~4.3) and Si (~3.5), and the free carrier absorption in the p- and n-layers was estimated using the Drude model as in Ref. 30. As in Fig. 1(b), the spectral absorption coefficient values of the $Ge/Si_{0.16}Ge_{0.84}$ MQWs at different electrical bias were extracted from the experimental data[26] using the same epitaxial structure. It should be noted that in MQWs, electric fields higher than the breakdown field of the bulk material can be possibly applied; due to the quantum confinement effect, the hole and electron wavefunctions are displaced from the band edges resulting in increased ionization energy.[13]

Figure 2(a) shows that the effective index of the quasi-TE fundamental mode can be smoothly transferred via the 2D taper from the $Si_{0.16}Ge_{0.84}$ waveguide to the $Ge/Si_{0.16}Ge_{0.84}$ MQW one; the corresponding optical mode of each effective index value can be seen in the inset of Fig. 2(a). To consider the taper fabrication tolerance, Figs. 2(b)–2(e) report on the optical coupling loss between the fundamental quasi-TE mode at the $Si_{0.16}Ge_{0.84}$ waveguide and the fundamental quasi-TE mode at the end of taper with respect to the variations in the taper tip width (a), taper length (L), taper end width (w), and $Si_{0.16}Ge_{0.84}$ rib waveguide's width at the end of taper (b). The coupling loss at 0 V bias can be as low as ~0.87 dB, and it is relatively robust against the variations in a, L, w, and b. The most critical parameter is the taper tip width of 0.7 μm, which is needed to avoid an abrupt disruption of the optical mode in the $Si_{0.16}Ge_{0.84}$ input waveguide. Positively, it still takes a variation of more than 100 nm (0.1 μm) to significantly affect the optical coupling performance, which should be within the capability of modern fabrication processes. In the simulation, the material absorption losses are included, and the absorption coefficient of $Ge/Si_{0.16}Ge_{0.84}$ MQWs is at 0 V (no electrical bias). Hence, the optical coupling loss due to both the difference in the effective refractive index between the $Si_{0.16}Ge_{0.84}$ and $Ge/Si_{0.16}Ge_{0.84}$ MQW waveguides and material absorption is properly taken into account. In FDTD simulations (Lumerical, Inc.), the smallest grid size is ~2 nm, and a perfectly matched layer (PML) is used in order to suppress reflections from the boundaries.

III. INTEGRATED MODULATION PERFORMANCE

Figure 3(a) reports on the optical propagation of the entire structure from the input $Si_{0.16}Ge_{0.84}$ waveguide, via the input 2D taper through the 70-μm-long $Ge/Si_{0.16}Ge_{0.84}$ MQWs (absorption coefficient when there is no electrical bias), via the output 2D taper to the output $Si_{0.16}Ge_{0.84}$ waveguide at the optical wavelength of 1430 nm. The electric field intensity profile is shown along the propagation direction at the center of the structure, demonstrating adiabatic optical coupling between the quasi-transverse-electric (TE) fundamental mode in the $Si_{0.16}Ge_{0.84}$ waveguide and that in the $Ge/Si_{0.16}Ge_{0.84}$ MQW waveguide via the 2D tapers. We consider only quasi-TE light because the QCSE from Ge/SiGe MQWs typically operates in a low-loss regime with a heavy-hole-related transition in which the absorption strength for quasi-TE light is significantly stronger.[31] Additionally, contrary to our previous work[26] and early works on hybrid Si evanescent electroabsorption modulator,[32] the proposed design also includes the optical modulation effect in the taper section. Our structure can benefit from the fact that the
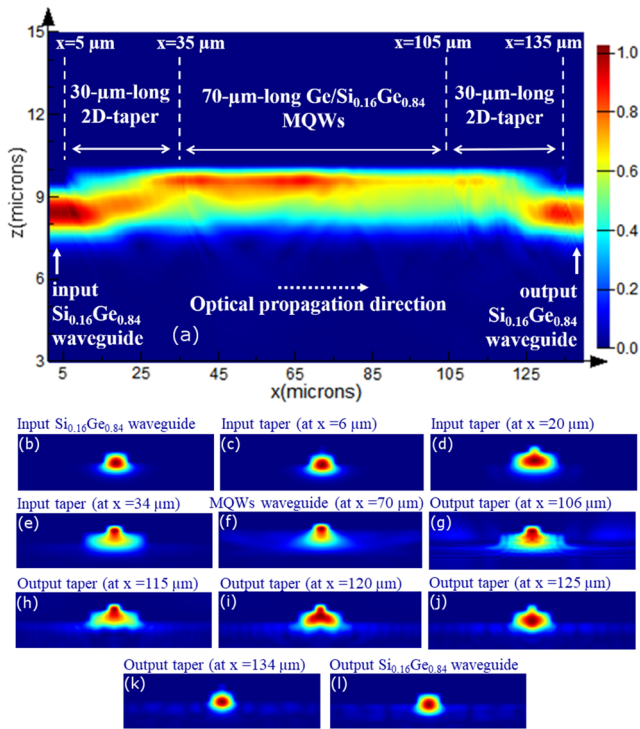
FIG. 3. (a) Optical propagation of the entire structure from the input $Si_{0.16}Ge_{0.84}$ waveguide via the input 2D taper through the 70-μm-long Ge/$Si_{0.16}Ge_{0.84}$ MQWs via the output 2D taper to the output $Si_{0.16}Ge_{0.84}$ waveguide at the optical wavelength of 1430 nm. The electric field intensity profile is shown along the propagation direction at the center of the structure. Cross-sectional electric field intensity profile at different positions of (b) input $Si_{0.16}Ge_{0.84}$ waveguide (c)–(e) input taper, (f) 70-μm-long Ge/$Si_{0.16}Ge_{0.84}$ MQWs, (g)–(k) output taper, and (l) output $Si_{0.16}Ge_{0.84}$ waveguide.

optical coupling is found to be adiabatic despite having a relatively wide taper, of which the narrowest section of 0.7 μm is still compatible to the width of previously demonstrated Ge/SiGe MQWs optical modulator;[19] therefore, one can reasonably expect that the taper section can be included without severely affecting the capacitance of the optical modulator. As in Fig. 3(a), the optical coupling from the fundamental quasi-TE mode of the $Si_{0.16}Ge_{0.84}$ waveguide

to that of the Ge/$Si_{0.16}Ge_{0.84}$ MQWs occurs throughout the length of the taper; hence, including optical modulation effect in the taper section will contribute to the achievable extinction ratio value from the device.

Figures 3(b)–3(l) show the cross-sectional electric field intensity profile at different positions. Figures 3(b)–3(e) re-affirm the results in Fig. 2 that the quasi-TE fundamental mode is adiabatically transferred from the input $Si_{0.16}Ge_{0.84}$ waveguide to the Ge/$Si_{0.16}Ge_{0.84}$ MQWs via the 2D taper. As in Fig. 3(f), the quasi-TE fundamental mode continues propagating in the straight Ge/$Si_{0.16}Ge_{0.84}$ MQW section, in which the p-layer is partially etched. Interestingly, 3D-FDTD simulation also reveals the stray light propagating in the partially etched p-layer slab. The stray light due to scattering is not unusual in photonic integrated circuits even when light encounters slight structural changes along the propagation direction, and it was shown that simple two bends could be used to have lateral offset necessary to sufficiently separate the stray light from the optical mode in Si-based photonic integrated circuits.[33] After propagating in the main Ge/$Si_{0.16}Ge_{0.84}$ MQW section, as expected, the quasi-TE fundamental mode is successfully transferred back from the Ge/$Si_{0.16}Ge_{0.84}$ MQWs to the output $Si_{0.16}Ge_{0.84}$ waveguide via the same 2D taper as in Figs. 3(g)–3(l). The scattering of light revealed in Fig. 3(g) is consistent with the fact that the partially etched p-type layer ends around that position. We also investigate the optical propagation at different optical wavelengths, electrical bias, and lengths of the straight Ge/$Si_{0.16}Ge_{0.84}$ MQW section (L_{MQWs}). For examples, Figs. 4(a)–4(d) show the optical propagation of the same structure as that in Fig. 3 at the optical wavelengths of 1420 nm, 1440 nm, 1460 nm, and 1480 nm, confirming that the coupling structure can be employed over the entire wavelengths suitable for low-loss operation, i.e., the wavelength longer than the excitonic peak.[18,31] The optical intensity at the output waveguide becomes higher with longer wavelength values, which is consistent with the lower absorption loss from the Ge/SiGe MQWs. Figures 4(e)–4(h) show examples of electric field intensity profiles from the same structure at different electrical bias from no electrical bias, ~6.1 × 10⁴, ~9.2 × 10⁴ to ~12.3 × 10⁴ V/cm, respectively. These values of electrical bias are corresponding to 0 V, 2 V, 3 V, and 4 V using 10 QW periods. The optical power at the output waveguide is lower at higher electrical bias, which is consistent with the characteristics of the Ge/$Si_{0.16}Ge_{0.84}$ MQWs as in Fig. 1(b), exhibiting redshift in their absorption spectra at higher electric fields. Figures 4(i)–4(l) show examples of electric field intensity
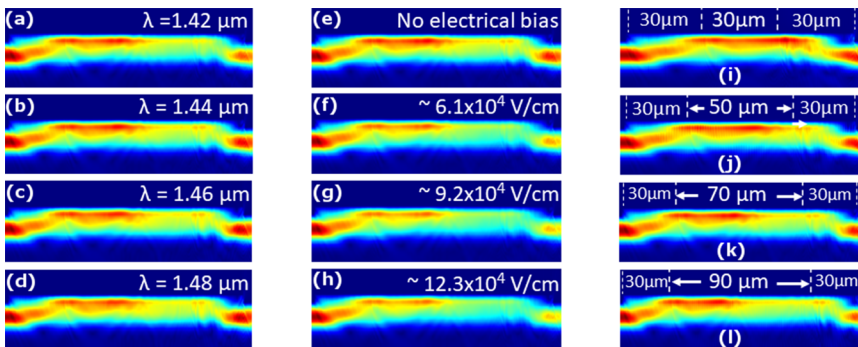

FIG. 4. Optical propagation of the same structure as that in Fig. 3 at (a)–(d) different optical wavelengths and (e)–(h) different electrical bias values. (i)–(l) Optical propagation at different L_{MQWs} values at the optical wavelength of 1430 nm with no electrical bias.

profiles at different L_{MQWs} values at the optical wavelength of 1430 nm at L_{MQWs} = 30 μm, 50 μm, 70 μm, and 90 μm with no electrical bias. The quasi-TE fundamental mode is transferred from the input $Si_{0.16}Ge_{0.84}$ waveguide to the $Ge/Si_{0.16}Ge_{0.84}$ MQWs and to the back to the output $Si_{0.16}Ge_{0.84}$ waveguide independent of the length L_{MQWs}; therefore, we can be assured that the optical coupling via the 2D taper is adiabatic-typed. The optical power at the output waveguide is lower with longer values of L_{MQWs}, which agree with the higher absorption length of the devices.

Figures 5(a)–5(d) report on the integrated extinction ratio (ER) and insertion loss (IL)[34] at various values of length L_{MQWs}, electrical bias, and optical wavelengths. The ER is defined as the ratio between the optical power values of the quasi-TE fundamental mode at the $Si_{0.16}Ge_{0.84}$ output waveguide with and without electrical bias as follows:

$$ER = 10 \cdot \log_{10}(I_{out,without\ bias}/I_{out,with\ bias}), \tag{1}$$

while the IL is the ratio between the optical power at the $Si_{0.16}Ge_{0.84}$ input waveguide and the optical power of the quasi-TE fundamental mode at the $Si_{0.16}Ge_{0.84}$ output waveguide without electrical bias as follows:

$$IL = 10 \cdot \log_{10}(I_{in}/I_{out,without\ bias}). \tag{2}$$

To be conservative, we do not include the power of stray light in the slab at the output as it is expected to leak away eventually. Both ER and IL increase with the length L_{MQWs} as expected. Significantly, as in Fig. 5(c), for a spectral range of ~20 nm between 1433 nm and 1453 nm, the values of waveguide-integrated ER is higher than the waveguide-integrated IL, i.e., ER/IL of ≥1, at L_{MQWs} = 70 μm with ~12.3 × 10⁴ V/cm (4 V for 10 QW periods.) Within the same wavelengths of interest, the reported IL values vary between only 3.1 dB and 3.8 dB, which can be considered relatively impressive as these IL values already include both the coupling loss of the two tapers and material absorption losses. For example, at 1441 nm, the ER of ~3.7 dB and IL of ~3.3 dB can be simultaneously obtained (waveguide-integrated ER/IL of ~1.1). To ensure that the simulation is well calibrated, it is worth mentioning that the performance reported in this work is consistent with the experimental results previously obtained from a fiber-coupled stand-alone device available in literature based on the same Ge/SiGe MQWs structure.[26] In Ref. 26, ~2.2 dB loss was measured from a 100-μm-long stand-alone Ge/SiGe MQWs, corresponding to ~0.022 dB per μm loss at the same optical wavelength of 1441 nm. This is clearly consistent with the IL ~3.3 dB obtained from this simulation of the SiGe waveguide-integrated device, which can be attributed to twice the ~0.87 dB loss from the two tapers and the ~1.54 dB (0.022 times 70) from the

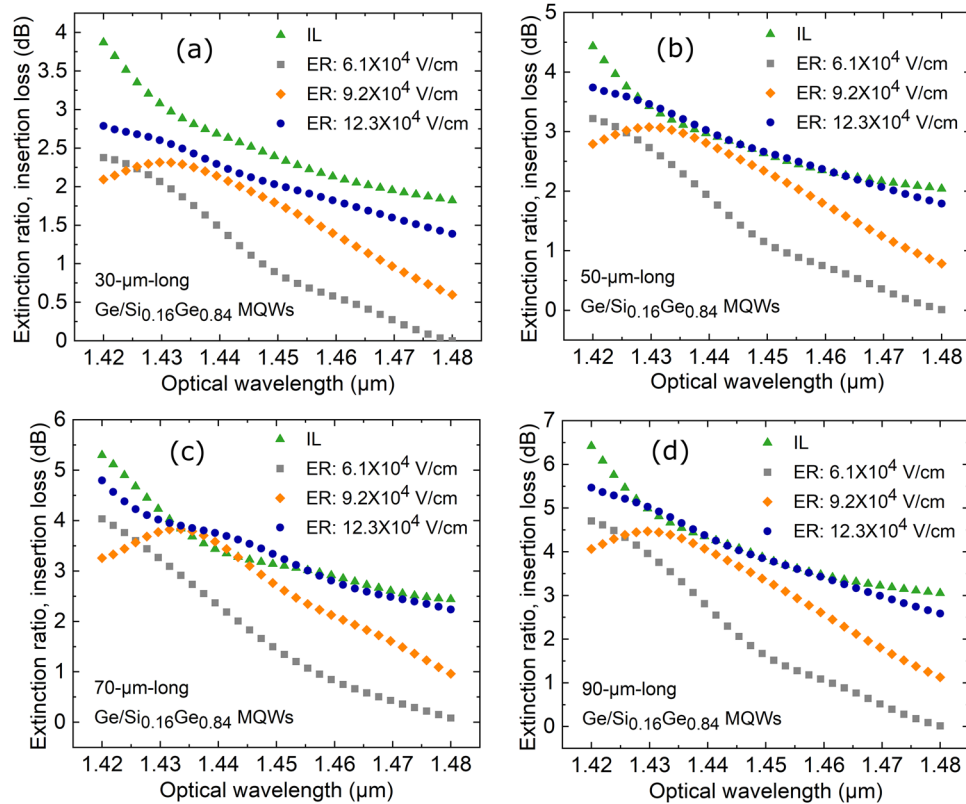**FIG. 5.** Spectral optical modulation performance of the $Si_{0.16}Ge_{0.84}$ waveguide integrated $Ge/Si_{0.16}Ge_{0.84}$ MQWs optical modulator with 10 QW periods in terms of integrated extinction ratio (ER) and insertion loss (IL) for L_{MQWs} = (a) 30, (b) 50, (c) 70, and (d) 90 μm, respectively, at various values of optical wavelengths and electrical bias.

70-μm-long straight waveguide region. For L_{MQWs} = 50 μm and 90 μm, the values of ER are also as high as IL for approximately the same spectral range region between 1433 nm and 1453 nm; nevertheless, we cannot obtain a region in which ER is evidently higher than IL. For L_{MQWs} = 30 μm, IL is higher than ER for all the wavelengths of interest at every electrical bias value; as the device is relatively short, the obtained optical modulation effect is still relatively low. It is important to note that the targeted integrated ER/IL of ≥1 in this simulation is consistent with the recent development of waveguide-integrated Ge-based optical modulators experimentally reported in the literature. For example, in SOI waveguide-integrated Ge Franz Keldysh (FK) optical modulators, Srinivasan et al.[35] reported ER and IL of 4.6 dB and 4.9 dB (ER/IL ~ 0.94) at the optical wavelength of 1615 nm (0 V–2 V bias), Feng et al.[36] reported ER and IL of 6 dB and 5 dB (ER/IL ~ 1.2) at the optical wavelength of 1550 nm (0 V–2.8 V bias), and Mastronardi et al.[37] reported ER and IL of 5.2 dB and 10.6 dB (ER/IL ~ 0.5) at the optical wavelength of 1566 nm (0 V–4 V bias). Last but not least, it should be noted that the typical optical loss due to the top and bottom metal contacts can be negligible in waveguide vertical p-i-n optical modulator as both metal contacts can be put laterally away from the optical modes.[38,39]

Significantly, in order to show the advantages and drawbacks of the designed optical modulator, Table I summarizes the comparison of the designed modulator with the published state-of-the-art Ge-based optical modulators. Besides the comparable values of ER/IL and driving voltage with Refs. 35–37 as aforementioned, the proposed solution can be developed on a bulk Si platform, which could be advantageous for monolithic integration with bulk Si electronics. Although a dedicated SiGe graded buffer on Si is needed to ensure high crystalline quality for the proposed device, it should be noted that the graded buffer platform has recently shown strong potential for wide usage in both communication and sensing applications.[40] The proposed solution also potentially enables a lower loss operation comparing to the QCSE-based device using a butt coupling approach with SOI waveguide.[19] Moreover, the QCSE-based device is nicely complementary to the existing FK-based ones as it can enable the operation in a shorter optical wavelength range into the S-band region, which is difficult to be attained using an FK-based device with acceptable absorption loss.[5]

To investigate the potential to further improve the waveguide-integrated ER and IL performance, we also explore the $Si_{0.16}Ge_{0.84}$

waveguide-integrated $Ge/Si_{0.16}Ge_{0.84}$ multi-quantum-well modulator with a different number of QW periods. As, respectively, shown in Figs. 6(a) and 6(b) at the optical wavelength of 1430 nm, the 2D taper can be adjusted to enable adiabatic optical coupling between the quasi-TE fundamental mode in the $Si_{0.16}Ge_{0.84}$ waveguide and the $Ge/Si_{0.16}Ge_{0.84}$ MQW waveguide with 15 and 20 QW periods. It is found that we can conveniently adjust only the taper end width (w) of the 2D taper to enable adiabatic optical coupling for different number of QWs, while the values of taper tip width (a), taper length (L), and $Si_{0.16}Ge_{0.84}$ rib waveguide's width at the end of the taper (b) can remain the same as those in the previous case of 10 QW periods. $Ge/Si_{0.16}Ge_{0.84}$ MQWs with a higher number of QW periods are found to require a narrower taper end width (w) to obtain a smooth transition of the effective index of the quasi-TE fundamental mode from the $Si_{0.16}Ge_{0.84}$ waveguide to the $Ge/Si_{0.16}Ge_{0.84}$ MQWs via the 2D taper. This is consistent with the fact that $Ge/Si_{0.16}Ge_{0.84}$ MQWs waveguide with a larger number of QWs will be thicker and are typically required to be narrower to obtain a comparable value of the effective index as that with a smaller number of QWs. It is also found that overall loss in the taper section is higher with a higher number of QWs because $Ge/Si_{0.16}Ge_{0.84}$ MQWs absorption losses in the taper region are also included. Figures 6(c)–6(f) show the values of ER and IL at different bias voltages over the spectral range of the QCSE suitable for low-loss operation. We focus on the lengths L_{MQWs} equal to 70 μm and 90 μm, which are found to render competitive values of waveguide integrated ER and IL in the previous case of 10 QWs. As in Fig. 6(c) with 15 QW periods and L_{MQWs} of 70 μm, waveguide-integrated ER is found to be higher than waveguide-integrated IL (ER/IL ≥ 1) for both electrical bias of ~9.2 × 10^4 V/cm (4 V for 15 QW periods) and ~12.3 × 10^4 V/cm (5.3 V for 15 QW periods) for a spectral range of ~10 nm between 1435 nm and 1445 nm and ~28 nm between 1435 nm and 1463 nm, respectively. For the electrical bias of ~12.3 × 10^4 V/cm, waveguide-integrated ER/IL of ≥1.1 can be maintained between 1441 nm and 1447 nm, and ER of ~4.5 dB and IL of ~4 dB can be simultaneously obtained. Therefore, by increasing the number of QWs to 15, the ER values can be increased at the expense of higher IL; nevertheless, ER/IL of ≥1 is still achievable. As in Figs. 6(d)–6(f), an increase in the straight $Ge/Si_{0.16}Ge_{0.84}$ MQW section length to 90 μm or in the QW periods to 20 would not improve the waveguide-integrated ER/IL performance. The region where the values of waveguide-integrated ER are

TABLE I. Comparison of the designed SiGe waveguide-integrated Ge/SiGe QCSE optical modulator with the recently published state-of-the-art works on Ge-based optical modulators.

| Reference	Ge-based device and waveguide	Footprint of active region (width × length μm^2)	Voltage swing (V)	Wavelength (nm)	ER/LL
35	Ge on Si SOI waveguide	0.6 × 40	0–2	1615	4.6 dB/4.9 dB (ER/IL ~0.94)
36	$Ge_{0.993}Si_{0.007}$ on Si, SOI waveguide	1 × 50	0–2.8	1550	6 dB/5 dB (ER/IL ~1.2)
37	$Ge_{0.985}Si_{0.015}$ on Si, SOI waveguide	1.5 × 40	0–4	1566	5.2 dB/10.6 dB (ER/IL ~0.5)
19	$Ge/Si_{0.15}Ge_{0.85}$ MQWs on Si SOI waveguide	0.8 × 10	3.5–4.5	1460	3 dB/15 dB (ER/IL ~0.2)
This work	$Ge/Si_{0.16}Ge_{0.84}$ MQWs on SiGe graded buffer SiGe waveguide	1.4 × 70	0–4	1441	3.7 dB/3.3 dB (ER/IL ~1.1)
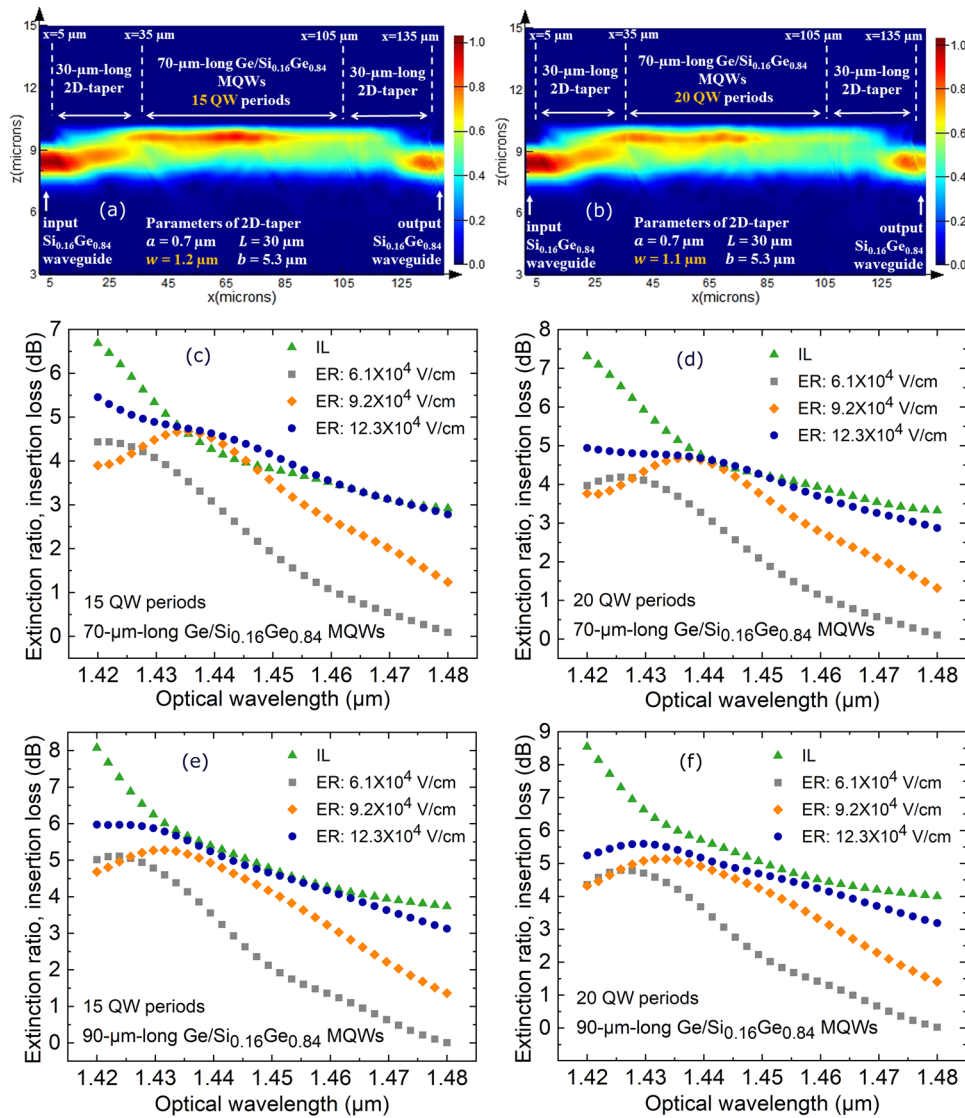
FIG. 6. Optical propagation of the entire structure of $Si_{0.16}Ge_{0.84}$ waveguide integrated $Ge/Si_{0.16}Ge_{0.84}$ MQWs optical modulator at the optical wavelength of 1430 nm with (a) 15 and (b) 20 QW periods. Spectral optical modulation performance in terms of integrated ER and IL for (c)–(d) L_{MQWs} = 70 and (e)–(f) L_{MQWs} = 90 μm for 15 and 20 QW periods at various values of optical wavelengths and electrical bias.

higher than the waveguide-integrated IL could not be obtained for the devices with L_{MQWs} of 90 μm as in Figs. 6(e) and 6(f) for both 15 and 20 QW periods. For the device with L_{MQWs} of 70 μm and 20 QW periods, the values of ER can be only as high as IL between 1441 nm and 1447 nm as in Fig. 6(d).

IV. CONCLUSIONS

We have reported the design and simulation of a waveguide-integrated Ge/SiGe QCSE optical modulator based on the use of a Ge-rich SiGe relaxed buffer on a SiGe graded buffer as a passive optical waveguide. Via 3D FDTD simulation, we have demonstrated

that potentially a simple 2D taper is sufficient to enable adiabatic optical coupling from the fundamental mode of the input SiGe waveguide to the fundamental mode of the Ge/SiGe MQWs modulator without the excitation of higher-order modes in Ge/SiGe MQWs with good fabrication tolerance. Significantly, the optical modulation performance of the SiGe waveguide-integrated Ge/SiGe QCSE optical modulator is investigated at different optical wavelengths, electrical bias values, device's length, and the number of quantum wells, and usable values of extinction ratio and insertion loss with respect to the recent development of waveguide-integrated Ge-based optical modulator in the literature can be simultaneously obtained.

DATA AVAILABILITY

The data that support the findings of this study are available from the corresponding author upon reasonable request.

REFERENCES

[1] Y.-H. Kuo, Y. K. Lee, Y. Ge, S. Ren, J. E. Roth, T. I. Kamins, D. A. B. Miller, and J. S. Harris, "Strong quantum-confined Stark effect in a germanium quantum-well structures on silicon," Nature **437**, 1334–1336 (2005).

[2] R. K. Schaevitz, J. E. Roth, S. Ren, O. Fidaner, and D. A. B. Miller, "Material properties of Si-SiGe quantum wells," IEEE J. Select. Top. Quantum Electron. **14**(4), 1082–1089 (2008).

[3] D. J. Paul, "8-band **k. p** modelling of the quantum confined Stark effect in Ge quantum wells on Si substrates," Phys. Rev. B **77**, 155323 (2008).

[4] L. Lever, Z. Ikonić, A. Valavanis, J. Cooper, and R. Kelsall, "Design of Ge-SiGe quantum-confined Stark effect electroabsorption heterostructures for CMOS compatible photonics," J. Lightwave Technol. **28**(22), 3273–3281 (2010).

[5] R. K. Schaevitz, E. H. Edwards, J. E. Roth, E. T. Fei, Y. Rong, P. Wahl, T. I. Kamins, J. S. Harris, and D. A. B. Miller, "Simple electroabsorption calculator for designing 1310 nm and 1550 nm modulators using germanium quantum wells," IEEE J. Quantum Electron. **48**, 187–197 (2012).

[6] M. Bonfanti, E. Grilli, M. Guzzi, D. Chrastina, G. Isella, H. von Känel, and H. Sigg, "Direct-gap related optical transitions in Ge/SiGe quantum wells with Ge-rich barriers," Physica E **41**, 972 (2009).

[7] P. Chaisakul, D. Marris-Morini, G. Isella, D. Chrastina, X. Le Roux, E. Gatti, S. Edmond, J. Osmond, E. Cassan, and L. Vivien, "Quantum-confined Stark effect measurements in Ge/SiGe quantum-well structures," Opt. Lett. **35**, 2913–2915 (2010).

[8] R. D. Kekatpure and A. Lentine, "The suitability of SiGe multiple quantum well modulators for short reach DWDM optical interconnects," Opt. Express **21**, 5318–5331 (2013).

[9] J. E. Roth, O. Fidaner, E. H. Edwards, R. K. Schaevitz, Y.-H. Kuo, N. C. Helman, T. I. Kamins, J. S. Harris, and D. A. B. Miller, "C-band side-entry Ge quantum well electroabsorption modulator on SOI operating at 1 volt swing," Electron. Lett. **44**, 49–50 (2008).

[10] E. H. Edwards, R. M. Audet, E. T. Fei, S. A. Claussen, R. K. Schaevitz, E. Tasyurek, Y. Rong, T. I. Kamins, J. S. Harris, and D. A. B. Miller, "Ge/SiGe asymmetric Fabry–Perot quantum well electroabsorption modulators," Opt. Express **20**, 29164–29173 (2012).

[11] R. M. Audet, E. H. Edwards, K. C. Balram, S. A. Claussen, R. K. Schaevitz, E. Tasyurek, Y. Rong, E. I. Fei, T. I. Kamins, J. S. Harris, and D. A. B. Miller, "Surface-normal Ge/SiGe asymmetric Fabry-Perot optical modulators fabricated on silicon substrates," J. Lightwave Technol. **31**, 3995–4003 (2013).

[12] P. Chaisakul, D. Marris-Morini, M.-S. Rouifed, G. Isella, D. Chrastina, J. Frigerio, X. Le Roux, S. Edmond, J.-R. Coudevylle, and L. Vivien, "23 GHz Ge/SiGe multiple quantum well electro-absorption modulator," Opt. Express **20**, 3219–3224 (2012).

[13] L. Lever, Y. Hu, M. Myronov, X. Liu, N. Owens, F. Y. Gardes, I. P. Marko, S. J. Sweeney, Z. Ikonić, D. R. Leadley, G. T. Reed, and R. W. Kelsall, "Modulation of the absorption coefficient at 1.3 μm in Ge/SiGe multiple quantum well heterostructures on silicon," Opt. Lett. **36**, 4158–4160 (2011).

[14] M. S. Rouifed, P. Chaisakul, D. Marris-Morini, J. Frigerio, G. Isella, D. Chrastina, S. Edmond, X. L. Roux, J.-R. Coudevylle, and L. Vivien, "Quantum-confined Stark effect at 1.3 μm in Ge/Si$_{0.35}$Ge$_{0.65}$ quantum-well structure," Opt. Lett. **37**, 3960–3962 (2012).

[15] J. Gao, H. Zhou, J. Jiang, Y. Zhou, and J. Sun, "Design of low bias voltage Ge/SiGe multiple quantum wells electro-absorption modulator at 1550 nm," AIP Adv. **7**, 035317 (2017).

[16] L. Lever, Z. Ikonić, and R. W. Kelsall, "Adiabatic mode coupling between SiGe photonic devices and SOI waveguides," Opt. Express **20**(28), 29500–29506 (2012).

[17] E. H. Edwards, L. Lever, E. T. Fei, T. I. Kamins, Z. Ikonic, J. S. Harris, R. W. Kelsall, and D. A. B. Miller, "Low-voltage broad-band electroabsorption from thin Ge/SiGe quantum wells epitaxially grown on silicon," Opt. Express **21**, 867–876 (2013).

[18] P. Chaisakul, J. Frigerio, D. Marris-Morini, V. Vakarin, D. Chrastina, G. Isella, and L. Vivien, "O-band quantum-confined Stark effect optical modulator from Ge/SiGe QWs by well thickness tuning," J. Appl. Phys. **116**(19), 193103 (2014).

[19] S. Ren, Y. Rong, S. A. Claussen, R. K. Schaevitz, T. I. Kamins, J. S. Harris, and D. A. B. Miller, "Ge/SiGe quantum well waveguide modulator monolithically integrated with SOI waveguides," IEEE Photonics Technol. Lett. **24**, 461–463 (2012).

[20] L. C. Kimerling, D.-L. Kwong, and K. Wada, "Scaling computation with silicon photonics," MRS Bull. **39**(8), 687–695 (2014).

[21] D. Thomson, A. Zilkie, J. E. Bowers, T. Komljenovic, G. T. Reed, L. Vivien, D. Marris-Morini, E. Cassan, L. Virot, J.-M. Fédéli, J.-M. Hartmann, J. H. Schmid, D.-X. Xu, F. Boeuf, P. O'Brien, G. Z. Mashanovich, and M. Nedeljkovic, "Roadmap on silicon photonics," J. Opt. **18**, 073003 (2016).

[22] X. Wang and J. Liu, "Emerging technologies in Si active photonics," J. Semicond. **39**, 061001 (2018).

[23] K. Zang, C.-Y. Lu, X. Chen, E. Fei, M. Xue, S. Claussen, M. Morea, Y. Chen, R. Dutt, Y. Huo, T. I. Kamins, and J. S. Harris, "Germanium quantum well QCSE waveguide modulator with tapered coupling in distributed modulator–detector system," J. Lightwave Technol. **35**(21), 4629–4633 (2017).

[24] M. Akie, T. Fujisawa, T. Sato, M. Arai, and K. Saitoh, "GeSn/SiGeSn multiple-quantum-well electroabsorption modulator with taper coupler for Mid-infrared Ge-on-Si platform," IEEE J. Sel. Top. Quantum Electron. **24**(6), 3400208 (2018).

[25] S. A. Srinivasan, C. Porret, E. Vissers, P. Favia, J. De Coster, H. Bender, R. Loo, D. Van Thourhout, J. Van Campenhout, and M. Pantouvaki, "High absorption contrast quantum confined Stark effect in ultra-thin Ge/SiGe quantum well stacks grown on Si," IEEE J. Quantum Electron. **56**(1), 5200207 (2020).

[26] P. Chaisakul, D. Marris-Morini, J. Frigerio, D. Chrastina, M.-S. Rouifed, S. Cecchi, P. Crozat, G. Isella, and L. Vivien, "Integrated germanium optical interconnects on silicon substrates," Nat. Photonics **8**, 482–488 (2014).

[27] H. Zhou, J. Sun, J. Gao, J. Jiang, and Y. Zhou, "Design of compact and efficient polarization-insensitive taper coupler for SiGe photonic integration," Opt. Express **24**(21), 23784–23797 (2016).

[28] G. Isella, D. Chrastina, B. Rössner, T. Hackbarth, H.-J. Herzog, U. König, and H. von Känel, "Low-energy plasma-enhanced chemical vapor deposition for strained Si and Ge heterostructures and devices," Solid State Electron. **48**, 1317–1323 (2004).

[29] V. Vakarin, P. Chaisakul, J. Frigerio, A. Ballabio, X. Le Roux, J.-R. Coudevylle, D. Bouville, D. Perez-Galacho, L. Vivien, G. Isella, and D. Marris-Morini, "Sharp bends and Mach-Zehnder interferometer based on Ge-rich-SiGe waveguides on SiGe graded buffer," Opt. Express **23**(24), 30821–30826 (2015).

[30] M. S. Rouifed, D. Marris-Morini, P. Chaisakul, J. Frigerio, G. Isella, D. Chrastina, S. Edmond et al., "Advances toward Ge/SiGe quantum-well waveguide modulators at 1.3 μm," IEEE J. Sel. Top. Quantum Electron. **20**(4), 33–39 (2014).

[31] P. Chaisakul, D. Marris-Morini, M. S. Rouifed, J. Frigerio, G. Isella, D. Chrastina, J.-R. Coudevylle, X. Le Roux, S. Edmond, D. Bouville, and L. Vivien, "Strong quantum-confined Stark effect from light hole related direct-gap transitions in Ge quantum wells," Appl. Phys. Lett. **102**(19), 191107 (2013).

[32] Y. Tang, H.-W. Chen, S. Jain, J. D. Peters, U. Westergren, and J. E. Bowers, "50 Gb/s hybrid silicon traveling-wave electroabsorption modulator," Opt. Express **19**(7), 5811–5816 (2011).

[33] R. Halir, A. Ortega-Moñux, í. Molina-Fernández, J. G. Wangüemert-Pérez, P. Cheben, D.-X. Xu, B. Lamontagne, and S. Janz, "Compact high-performance multimode interference couplers in silicon-on-insulator," IEEE Photonics Technol. Lett. **21**(21), 1600–1602 (2009).

[34]W. Traiwattanapong, K. Wada, and P. Chaisakul, "Analysis of optical integration between Si₃N₄ waveguide and a Ge-based optical modulator using a lateral amorphous GeSi taper at the telecommunication wavelength of 1.55 μm," Appl. Sci. **9**(18), 3846 (2019).

[35]S. A. Srinivasan, M. Pantouvaki, S. Gupta, H. T. Chen, P. Verheyen, G. Lepage, G. Roelkens, K. Saraswat, D. Van Thourhout, P. Absil, and J. Van Campenhout, "56 Gb/s germanium waveguide electro-absorption modulator," J. Lightwave Technol. **34**(2), 419–424 (2016).

[36]D. Feng, S. Liao, H. Liang, J. Fong, B. Bijlani, R. Shafiiha, B. J. Luff, Y. Luo, J. Cunningham, A. V. Krishnamoorthy, and M. Asghari, "High speed GeSi electro-absorption modulator at 1550 nm wavelength on SOI waveguide," Opt. Express **20**(20), 22224–22232 (2012).

[37]L. Mastronardi, M. Banakar, A. Z. Khokhar, N. Hattasan, T. Rutirawut, T. D. Bucio, K. M. Grabska, C. Littlejohns, A. Bazin, G. Mashanovich, and

F. Y. Gardes, "High-speed Si/GeSi hetero-structure electro absorption modulator," Opt. Express **26**(6), 6663–6673 (2018).

[38]J. Liu, M. Beals, A. Pomerene, S. Bernardis, R. Sun, J. Cheng, L. C. Kimerling, and J. Michel, "Waveguide-integrated, ultralow-energy GeSi electro-absorption modulators," Nat. Photonics **2**(7), 433–437 (2008).

[39]J. P. van Engelen, L. Shen, G. Roelkens, Y. Jiao, M. K. Smit, and J. J. G. M. van der Tol, "A novel broadband electro-absorption modulator based on bandfilling in n-InGaAs: Design and simulations," IEEE J. Sel. Top. Quantum Electron. **24**(1), 3300108 (2018).

[40]D. Marris-Morini, V. Vakarin, J. M. Ramirez, Q. Liu, A. Ballabio, J. Frigerio, M. Montesinos, C. Alonso-Ramos, X. Le Roux, S. Serna, D. Benedikovic, D. Chrastina, L. Vivien, and G. Isella, "Germanium-based integrated photonics from near- to mid-infrared applications," Nanophotonics **7**(11), 1781–1793 (2018).